nature physics

LETTERS

https://doi.org/10.1038/s41567-021-01355-4

Check for updates

Quantum coherent spin–electric control in a molecular nanomagnet at clock transitions

Junjie Liu[1]✉, Jakub Mrozek[1], Aman Ullah[2], Yan Duan[2], José J. Baldoví[2], Eugenio Coronado[2], Alejandro Gaita-Ariño[2]✉ and Arzhang Ardavan[1]✉

Electrical control of spins at the nanoscale offers significant architectural advantages in spintronics, because electric fields can be confined over shorter length scales than magnetic fields[1–5]. Thus, recent demonstrations of electric-field sensitivities in molecular spin materials[6–8] are tantalizing, raising the viability of the quantum analogues of macroscopic magneto-electric devices[9–15]. However, the electric-field sensitivities reported so far are rather weak, prompting the question of how to design molecules with stronger spin–electric couplings. Here we show that one path is to identify an energy scale in the spin spectrum that is associated with a structural degree of freedom with a substantial electrical polarizability. We study an example of a molecular nanomagnet in which a small structural distortion establishes clock transitions (that is, transitions whose energy is to first order independent of the magnetic field) in the spin spectrum; the fact that this distortion is associated with an electric dipole allows us to control the clock-transition energy to an unprecedented degree. We demonstrate coherent electrical control of the quantum spin state and exploit it to independently manipulate the two magnetically identical but inversion-related molecules in the unit cell of the crystal. Our findings pave the way for the use of molecular spins in quantum technologies and spintronics.

The polyoxometalate molecular anion $[Ho(W_5O_{18})_2]^{9-}$ (abbreviated to HoW_{10}), within the crystal structure $Na_9[Y_{1-x}Ho_x(W_5O_{18})_2]\cdot 35H_2O$ ($x=0.1\%$), provides an example of clock-transition (CT) molecular spin qubit[16,17]. In the solid state, the sodium salt of this anion crystallizes in a primitive space group of $P\bar{1}$, where each unit cell contains two HoW_{10} anions that are related via inversion symmetry. Each HoW_{10} possesses an approximate D_{4d} symmetry. The magnetic properties of HoW_{10}, which are characterized by a total electronic angular momentum of $J=8$ and a nuclear spin of $I=7/2$, can be described by the Hamiltonian[18]

$$H = \sum_{k=2,4,6}\sum_{q=-k}^{k} B_k^q O_k^q + J\cdot A\cdot I + \mu_B g_e \mathbf{B}_0\cdot J - \mu_N g_N \mathbf{B}_0\cdot I \quad (1)$$

where A is the magnitude of the (approximately) isotropic hyperfine interaction; g_e and g_N are the electronic and nuclear gyromagnetic ratios respectively; the anisotropy is parameterized by the amplitudes B_k^q of the extended Stevens operators O_k^q; and $\mathbf{B}_0$ is the applied magnetic field.

The crystal field terms $\sum_k B_k^0 O_k^0$ lead to a ground state of $m_J=\pm 4$, where m_J is the projection of the electronic angular momentum. Crucially, owing to interactions of HoW_{10} with counterions and crystallization water, there is a minor deviation from the ideal D_{4d} symmetry, with a continuous-shape measurement $S<0.1$ around the Ho^{3+} ion as defined by the SHAPE program[19] (Supplementary Information provides detailed information on methods, calculations and ancillary experiments). Specifically, the chemical structure shows that the skew angle, θ, deviates from the ideal value of 45°, and that the Ho^{3+} centre deviates from the centre position by a distance of $d=(h-h')/2$. The latter indicates that Ho^{3+} is closer to one of the two $[W_5O_{18}]^{6-}$ moieties. The crystal structures measured at three different temperatures (100, 150 and 200 K) are provided in Supplementary Information. At these three temperatures, deviations in the skew angles are 2.21°, 2.34° and 2.27°, and the off-centre distances are 0.021, 0.025 and 0.024 Å, respectively.

This gives rise to an electric dipole moment and a tetragonal spin anisotropy (parameterized by terms B_k^4), which mixes the $m_J=\pm 4$ ground states and generates a series of anticrossings in the spin spectrum, leading to four electron spin resonance (ESR) CTs, whose resonance frequencies are determined by the amplitude of tetragonal anisotropy. The four CTs correspond to resonances with different electron–nuclear spin states $|m_J, m_I\rangle$ with $m_J=\pm 4$ and $m_I=-1/2$, $-3/2$, $-5/2$ or $-7/2$ (from low to high fields). Previous ESR and magnetization studies[17,18] are satisfactorily simulated by the parameters $B_2^0/h=18.00\times 10^3$ MHz, $B_4^0/h=209.00$ MHz, $B_6^0/h=1.53$ MHz, $B_4^4/h=94.20$ MHz, $A/h=830.00$ MHz and $g_e=1.25$.

Thus, the broken inversion symmetry causes the spin–electric-coupled phenomena of an electric dipole and a CT. This, in turn, allows us to linearly manipulate the CT frequency by applying an external electric field (E field).

We investigated the spin–electric coupling (SEC) in HoW_{10} by embedding E-field pulses in an ESR Hahn-echo sequence, as described in ref. [6], Methods and Supplementary Information. Figure 1c shows typical data recorded with the E field applied parallel to $\mathbf{B}_0$ at $\varphi=0$. The in-phase part of the spin echo shows a pronounced oscillation on varying the length of the E-field pulse. The oscillation arises because the molecular spin Hamiltonian is modulated by the E field via the SEC, leading to a shift δf in the ESR frequency while the E field is applied. This shift in the ESR frequency manifests as an additional phase of $\delta f\times t_E$ in the spin echo signal, causing the oscillation with a period of 1 μs in the echo amplitude (Supplementary Fig. 1). The decay in the echo amplitude over $0<t_E\leq 6$ μs is due to a small inhomogeneity in the E field across the crystal; during the second period of free evolution, namely, $6<t_E\leq 12$ μs, the inhomogeneity is refocused and the echo amplitude recovers[6].

The lack of a dependence of the quadrature channel of the echo on t_E is evidence of a linear—as opposed to quadratic—SEC in

[1]CAESR, Department of Physics, University of Oxford, The Clarendon Laboratory, Oxford, UK. [2]Instituto de Ciencia Molecular (ICMol), Universitat de València, Paterna, Spain. ✉e-mail: junjie.liu@physics.ox.ac.uk; alejandro.gaita@uv.es; arzhang.ardavan@physics.ox.ac.uk

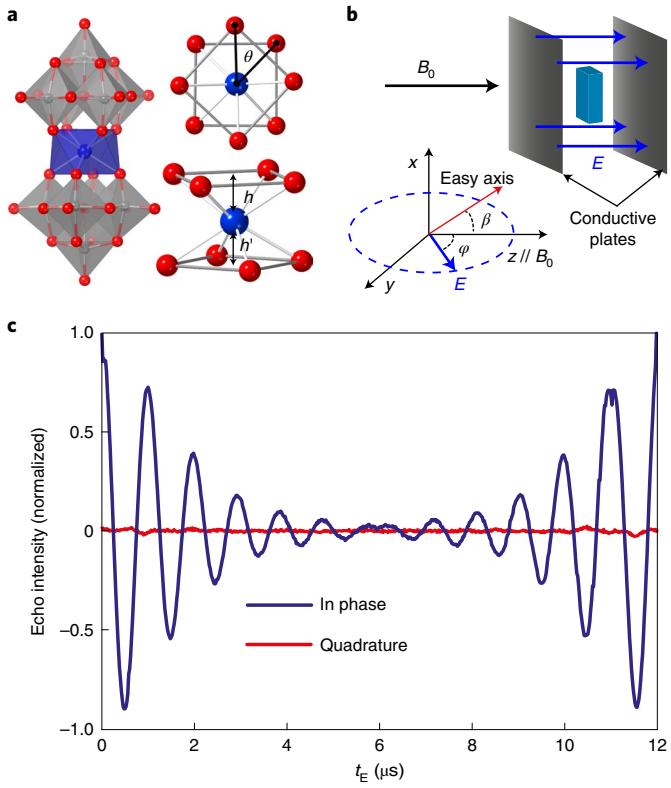

Fig. 1 | The spin–electric coupling experiment. A small rotation of the two Ho-coordinated $[W_5O_{18}]^{6-}$ ligands ($\theta \neq 45°$) and displacement of Ho ($h \neq h'$) give rise to a tetragonal anisotropy. **a**, HoW_{10} (left) and the coordination environment for the Ho^{3+} (right). **b**, Schematic showing the experimental configuration. The electric field was generated by applying voltage pulses to two parallel conducting plates. The magnetic field was applied parallel to the *z* axis (in the *x*–*y*–*z* laboratory frame). The sample was oriented to minimize the angle between the molecular easy axis (the red arrow in the *x*–*z* plane) and $\mathbf{B}_0$ (estimated misalignment, $\beta \approx 38°$). The *E*-field orientation φ was rotated within the *y*–*z* plane. **c**, *E*-field effect on the spin echo of HoW_{10} measured at $\mathbf{B}_0 = 0.0304$ T. The in-phase part of the integrated echo intensity strongly oscillates as a function of duration (t_E) of the *E*-field pulse generated by applying a voltage of 300 V. By comparison, the quadrature component (red line) remains flat at zero throughout the experiment. The durations of the $\pi/2$ and π microwave pulses were 32 and 64 ns, respectively, and the separation between them was fixed at 6 μs. All the SEC measurements presented in this work (except the selective spin excitation data shown in Fig. 3) were conducted using the same protocol and the shift in the ESR frequency, δf, is obtained by the Fourier transformation of the oscillating in-phase component of the spin echo.

HoW_{10}. The crystal unit cell contains two HoW_{10} units related by inversion symmetry; a linear SEC shifts the ESR frequency of each by the same amount but in opposite directions. Hence, the phase shifts for the spin echoes of the two inequivalent spins are $+\delta f \times t_E$ and $-\delta f \times t_E$ and the quadrature part of the combined echo signal remains zero, independent of t_E. For a second-order SEC $\delta f \propto E^2$, both spins in the unit cell acquire the same phase, because the shift is insensitive to the polarity of the *E* field. Thus, an oscillation in the quadrature component—$\pi/2$ out of phase with the in-phase component—is a signature of a second-order SEC. (An oscillation in the quadrature component can also arise if the *E*-field pulse is accompanied by a parasitic magnetic field pulse that distorts $\mathbf{B}_0$; it contributes a trivial phase to the echo via the Zeeman interaction.)

The orientation dependence of the SEC is shown in Fig. 2a. The shift in ESR frequency (δf) is calculated by taking the fast Fourier transform of the oscillation in the in-phase echo intensity. It depends on orientation as $|\delta f| \propto |\cos(\varphi - \varphi_0)|$ (the presence of both inversion-related populations means that we cannot distinguish the sign of δf from this measurement). This yields a lower bound on the scale of the SEC; a full mapping of the SEC orientation dependence would be required to establish the orientation with the maximum *E*-field sensitivity. This would depend on the two-axis rotation of the electric field, which is beyond the scope of this study.

The linearity of the SEC is further confirmed by varying the amplitude of an *E*-field pulse with fixed duration. Figure 2b demonstrates that the frequency shift is proportional to the voltage (and hence, since the electrode geometry is fixed, the amplitude of the *E* field). The data were recorded at orientation φ that shows the strongest SEC. The linear fit to the data yields a SEC constant of $11.4 \pm 0.3\,\mathrm{Hz\,(V\,m^{-1})^{-1}}$.

The relative strength of the SEC in HoW_{10} showcases the potential for chemical design in enhancing the desired molecular properties via a prudent choice of the coordination environment of the metal ion. Such engineering is not possible in, for example, atomic defects in solid state materials, in which structures and therefore properties are much less tunable. Furthermore, the possibility of tuning the ESR transition at the CT fields allows the exploitation of the strong spin–orbit coupling characteristic of 4*f* electrons to enhance the electrical control of molecular qubits while retaining substantial coherence times. Such tuning of the HoW_{10} CT can only be efficiently achieved by directly adjusting the tetragonal anisotropy interaction since at the CT fields, the ESR transitions are insensitive to g_e or *A* to first order (Supplementary Information).

The ESR frequency at the CT fields is determined by the tetragonal anisotropy. Therefore, all ESR transitions at 9.15 GHz exhibit the same response to the applied electric fields (filled squares in Fig. 2d) and can be fitted with $\delta B_4^4/h = (8.8 \pm 0.2) \times 10^{-3}\,\mathrm{MHz}$ $(5.9 \times 10^{-2}\,\mathrm{Hz\,(V\,m^{-1})^{-1}})$. However, other spin Hamiltonian terms, such as Zeeman and hyperfine interactions, may potentially also exhibit *E*-field sensitivities. These interactions modify the ESR transition frequencies away from the CT fields; we can probe their sensitivities by studying the *E*-field effect on ESR transitions away from the CT fields, as shown in Fig. 2c,d.

The *E*-field-induced ESR frequency shift decreases as the ESR frequency increases, which is expected as the 'anticrossing' effect of B_4^4 reduces when moving away from the CTs. On the other hand, the SEC effects also fluctuate considerably from peak to peak at 9.45 and 9.88 GHz. Such fluctuation is likely due to the *E*-field modulation of Hamiltonian parameters other than B_4^4: the appreciable dependence of δf on the magnetic field and nuclear spin projection away from the CT fields (that is, between the states with varying contributions from different nuclear spin projections m_I and electron spin projections m_J) suggest that Zeeman and hyperfine interactions may also be sensitive to the *E* field, though less than B_4^4 (Supplementary Information).

We seek insight into the relationship between the *E*-field-induced distortion and CT frequency by noting that any molecular distortion may be decomposed into displacements of the normal modes of HoW_{10}, which we obtain using density functional theory (DFT, implemented by Gaussian[20]). Each normal mode is associated with force constant κ_i and reduced mass μ_i (yielding eigenfrequency $\omega_i = \sqrt{\kappa_i/\mu_i}$). The electric dipole $\mathbf{p}$ depends on the displacement of mode x_i, and this determines the coupling of the mode to an applied *E* field or to incident light, that is, its infrared intensity.

When an external electric field $\mathbf{E}$ is incremented by $\mathrm{d}\mathbf{E}$, it elastically distorts the molecule by $\mathrm{d}x_i$ and modifies the molecular electric dipole by $\mathrm{d}\mathbf{p}_i$ for mode *i*. In this process, it does work $\mathbf{E} \cdot \sum_i \mathrm{d}\mathbf{p}_i = \sum_i \kappa_i \mathrm{d}x_i$. Thus, by calculating the electric dipole moment as a function of the mode displacements, we can quantitatively

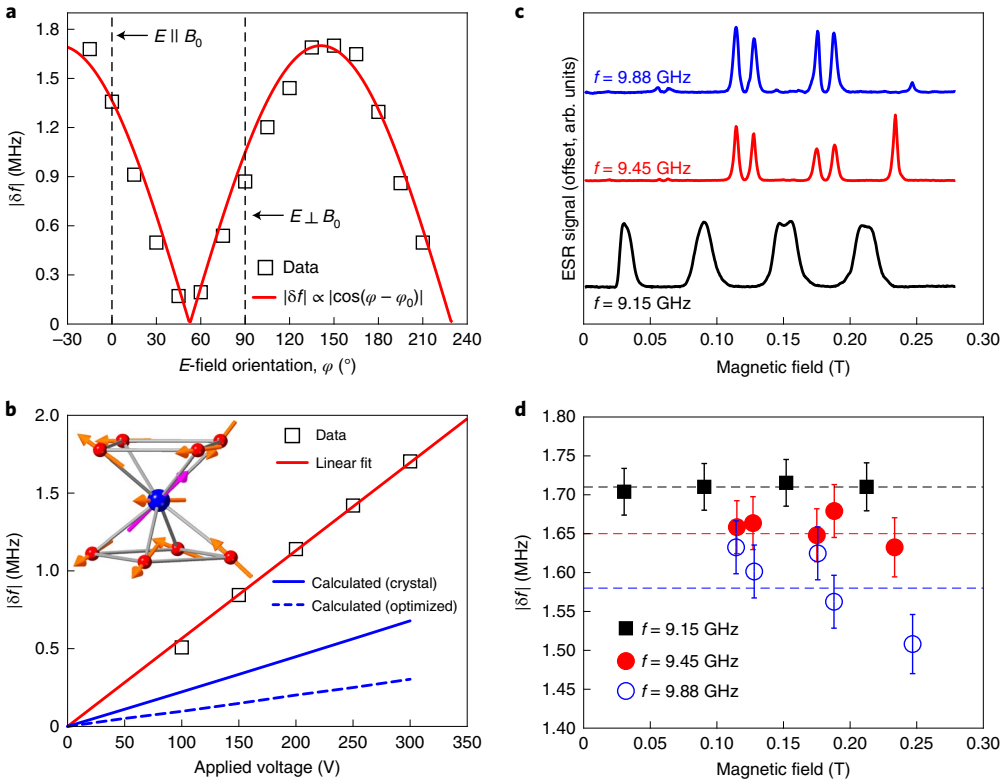

Fig. 2 | SEC dependence on orientation, *E* field and magnetic field. a, Orientation dependence of the *E*-field-induced frequency shift. The measurements were performed at $f = 9.15$ GHz, $V = 300$ V and $\mathbf{B}_0 = 0.0304$ T. The *E* field was rotated between being parallel to $\boldsymbol{B}_0$ (that is, 38° away from the molecular easy axis) at $\varphi = 0°$ (180°) and perpendicular to $\mathbf{B}_0$ (that is, in the molecular hard plane) at $\varphi = 90°$. **b**, Measured frequency shift (squares) versus applied voltage *V*, showing a linear *E*-field coupling in HoW_{10}. The data were recorded at the orientation with the strongest SEC ($\varphi = 145°$). The red line is a linear fit to the data. The blue lines represent the ab initio prediction based on molecular geometry extracted from (solid) single-crystal X-ray crystallography or (dashed) structure fully optimized at the DFT level (Supplementary Information). Inset: the local environment of Ho showing the electric dipole direction (magenta arrow) and the *E*-field-induced atomic displacement directions (orange arrows). **c**, ESR spectra recorded at various frequencies close to the CT frequency. **d**, The *E*-field effect measured on the corresponding ESR transitions. Error bars indicate the full-width at half-maximum of the Fourier transform of the in-phase echo signal. The dashed lines illustrate the *E*-field-induced frequency shift δf expected if only B_4^4 were modified by the *E* field; the scatter in δf at frequencies away from the CT indicates that the *E*-field sensitivity of other Hamiltonian terms becomes important. The error bars for δf in **a** and **b** are approximately equal to the size of the symbols (not shown).

extract the displacements as a function of the applied *E* field and hence the *E*-field-induced evolution of the molecular electronic structure (Methods).

This reasoning yields the criteria by which we may determine whether a particular molecular mode leads to a strong contribution to the SEC at the CT frequency: it should be relatively soft (that is, small κ_i), allowing a substantial molecular displacement without excessive elastic energy cost; it should strongly couple to the molecular electric dipole (that is, $d\mathbf{p}_i/dx_i$, and therefore its infrared intensity, should be large); and it should modify the Ho environment such that the energy of the anticrossing levels is modulated. Our analysis of the basis of the HoW_{10} vibrational modes of the crystallographic structure reveals that the molecular displacement responsible for the SEC can be approximated by the distortion displacing the Ho and coordinating oxygen atoms, as shown in Fig. 2b, inset. The analysis based on the relaxed structure yields a very similar result. Animations showing each of these collective distortions are available in the Supplementary Information. The difference between the SECs predicted using the optimized and crystal structures (blue dashed/solid lines in Fig. 2b) can be understood by considering how the structure deviates from the ideal D_{4d} symmetry. A departure from the D_{4d} structure, which is inversion symmetric, is necessary to afford a linear SEC in HoW_{10}. Compared with the optimized molecular geometry, the actual crystal structure shows a larger distortion due to the presence of Na^+ counterions and crystallization of H_2O molecules. Therefore, it is conceivable that the optimized structure leads to an underestimation of the SEC. Nevertheless, the theoretical results are in reasonable agreement with the experimental data.

We note in passing that from a practical perspective, any external electric field that can be experimentally applied is very small compared with the intramolecular fields associated with chemical bonds, justifying our perturbative approach. Others have investigated the effects of electric fields on the scale of ~10 V nm^{-1} on lanthanide single-ion molecular magnets, a regime that can be directly explored in DFT[21].

Finally, we demonstrate a protocol to selectively manipulate the spins of inversion-related HoW_{10} anions assisted by an *E* field[1,3]. Since the two spins within the unit cell are related by inversion symmetry, they are magnetically identical and cannot be distinguished in conventional ESR or magnetometry experiments. However, they exhibit opposite frequency shifts in the presence of an *E* field, which can be exploited, using a modified Hahn-echo sequence, as shown in Fig. 3a, to excite them selectively. The first pulse—a $\pi/2$ pulse at the CT frequency of $f_0 = 9.15$ GHz—places all molecular spins in the superposition state. An *E* field is applied simultaneously with the refocusing π pulse, lifting the degeneracy of the ESR transitions in the two inversion-related populations. Thus, it is possible to refocus

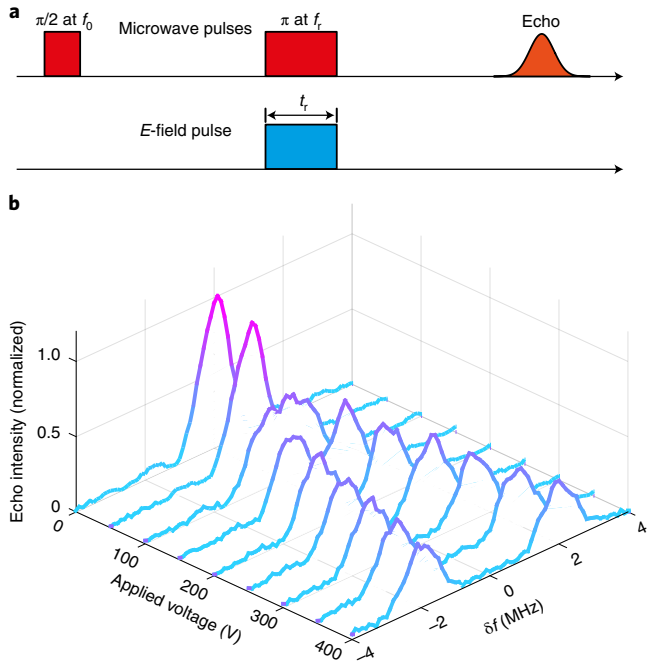

Fig. 3 | *E* field selection of molecular subpopulations. a, Modified Hahn-echo pulse sequence used for selective spin excitation. A $\pi/2$ pulse is applied at CT frequency f_0, while the frequency of the refocusing π pulse, f_r, is swept. An *E*-field square pulse is applied along with the refocusing pulse to modulate the excitation frequencies of molecular spins. When $f_r = f_0 \pm \delta f$, the refocusing pulse selectively inverts one or other of the inversion-symmetry-related molecular spins in the unit cell. **b**, Intensity of the spin echo as a function of the applied voltage, V, and the frequency offset of the refocusing pulse, $\delta f = f_0 - f_r$.

only one subpopulation, as long as (1) the π pulse is resonant with the shifted ESR frequency of that subpopulation and (2) the shift is larger than the natural line width of the excited spin population. The echo that forms following the second period of free evolution is detected at frequency f_0, but only comprises spins from the refocused subpopulation.

We set the durations of the $\pi/2$ and π microwave pulses to be 400 and 800 ns, respectively, to selectively excite a narrow frequency population of spins (note that these pulses are more than ten times longer than those used in the preceding experiments and therefore drive a correspondingly narrower range of ESR transition frequencies). Figure 3b shows a plot of the echo amplitude as a function of applied voltage V and frequency offset of the refocusing pulse $\delta f = f_0 - f_r$ (the Supplementary Information provides more data). In the absence of an *E*-field pulse ($V = 0$), the maximum echo signal is observed when the frequencies of the $\pi/2$ and π pulses are identical, that is, $\delta f = 0$. On increasing the amplitude of the *E* field, subpopulations are refocused for two different values of δf, and these subpopulations are spectrally well resolved for $V > 150$ V.

The offset is in excellent agreement with the expected SEC for HoW_{10} and the echo signal peaks at the symmetric positions $\pm\delta f$ around $\delta f = 0$, corresponding to the selective refocusing of the inversion-related subpopulations. Furthermore, the echo intensities at $\pm\delta f$ are identical and approximately half the intensity in the absence of an electric field, indicating that only half the population is refocused and that refocusing is equally effective for both subpopulations. This demonstrates that with the assistance of an *E* field, we can distinguish orientations of otherwise magnetically identical HoW_{10} units.

As is generally the case in quantum information experiments, strong coupling to a control field means strong coupling to a source of noise that shares the same physics as the control. In the case described here, we reduce the sensitivity to magnetic fields by working at a CT, but this, in turn, increases the sensitivity to molecular distortions and *E*-field fluctuations. We note, however, that reducing the temperature (which, will—in any case—be required for initialization) suppresses environmental phonons (the principal source of molecular distortions), but cannot remove all magnetic field fluctuations, which may have their origin in, for example, environmental spin flip-flop processes[22].

Our results guide us to distil the general recipe for a high-SEC molecule: a soft and electrically polarizable environment for the spin carriers, and a spin spectrum that is highly sensitive to distortions. These principles are satisfied in HoW_{10}, where a CT frequency is modulated by soft modes that shift the molecular charge distribution. The SEC is about an order of magnitude larger than the previously reported values for transition-metal-based molecular nanomagnets[6,7,23] ($\delta f/E < 1\,\mathrm{Hz\,m\,V^{-1}}$) and it also surpasses the SEC measured for rare-earth atoms doped in YAG (ref. [24]) ($\delta f/E \approx 1\,\mathrm{Hz\,m\,V^{-1}}$). It is similar to the SEC for Mn^{2+} in ZnO (ref. [25]) ($\delta f/E$ up to 12.7 Hz$(\mathrm{V\,m^{-1}})^{-1}$), in which the SEC is associated with the piezoelectric nature of the host lattice. The HoW_{10} coupling is sufficiently strong that a modest *E* field of $\sim 10^5\,\mathrm{V\,m^{-1}}$ or $100\,\mu\mathrm{V\,nm^{-1}}$ is adequate to tune the spin at a practically useful level, that is, to shift the frequency by much more than the natural line width; this demonstrates the principle that local *E*-field tuning allows for the selective addressing of spins in otherwise identical molecules. The strong SEC in HoW_{10} raises the tantalizing possibility of engineering a coherent spin–photon interface in molecular spintronic devices[26], allowing coherent spin control by an oscillating electric field[5]. These results pave the way for the use of molecular components in quantum or classical spintronic technologies in which local electrical control can surpass the performance of conventional magnetic spin control.

Online content

Any methods, additional references, Nature Research reporting summaries, source data, extended data, supplementary information, acknowledgements, peer review information; details of author contributions and competing interests; and statements of data and code availability are available at https://doi.org/10.1038/s41567-021-01355-4.

Received: 11 May 2020; Accepted: 13 August 2021;
Published online: 14 October 2021

References

1. Kane, B. E. A silicon-based nuclear spin quantum computer. *Nature* **393**, 133–137 (1998).
2. Trif, M., Troiani, F., Stepanenko, D. & Loss, D. Spin-electric coupling in molecular magnets. *Phys. Rev. Lett.* **101**, 217201 (2008).
3. Laucht, A. et al. Electrically controlling single-spin qubits in a continuous microwave field. *Sci. Adv.* **1**, e1500022 (2015).
4. Tosi, G. et al. Silicon quantum processor with robust long-distance qubit couplings. *Nat. Commun.* **8**, 450 (2017).
5. Asaad, S. et al. Coherent electrical control of a single high-spin nucleus in silicon. *Nature* **579**, 205–209 (2020).
6. Liu, J. et al. Electric field control of spins in molecular magnets. *Phys. Rev. Lett.* **122**, 037202 (2019).
7. Fittipaldi, M. et al. Electric field modulation of magnetic exchange in molecular helices. *Nat. Mater.* **18**, 329–334 (2019).
8. Robert, J., Parizel, N., Turek, P. & Boudalis, A. K. Polyanisotropic magnetoelectric coupling in an electrically controlled molecular spin qubit. *J. Am. Chem. Soc.* **141**, 19765–19775 (2019).
9. Palii, A., Clemente-Juan, J. M., Tsukerblat, B. & Coronado, E. Electric field control of the optical properties in magnetic mixed-valence molecules. *Chem. Sci.* **5**, 3598–3602 (2014).
10. Cardona-Serra, S. et al. Electrically switchable magnetic molecules: inducing a magnetic coupling by means of an external electric field in a mixed-valence polyoxovanadate cluster. *Chem. Eur. J.* **21**, 763–769 (2015).

11. Gaita-Ariño, A., Luis, F., Hill, S. & Coronado, E. Molecular spins for quantum computation. *Nat. Chem.* **11**, 301–309 (2019).
12. Atzori, M. & Sessoli, R. The second quantum revolution: role and challenges of molecular chemistry. *J. Am. Chem. Soc.* **141**, 11339–11352 (2019).
13. Godfrin, C. et al. Operating quantum states in single magnetic molecules: implementation of Grover's quantum algorithm. *Phys. Rev. Lett.* **119**, 187702 (2017).
14. Eerenstein, W., Mathur, N. D. & Scott, J. F. Multiferroic and magnetoelectric materials. *Nature* **442**, 759–765 (2006).
15. Matsukura, F., Tokura, Y. & Ohno, H. Control of magnetism by electric fields. *Nat. Nanotechnol.* **10**, 209–220 (2015).
16. AlDamen, M. A. et al. Mononuclear lanthanide single molecule magnets based on the polyoxometalates $[Ln(W_5O_{18})_2]^{9-}$ and $[Ln(\beta_2\text{-}SiW_{11}O_{39})_2]^{13-}$ (Ln^{III} = Tb, Dy, Ho, Er, Tm, and Yb). *Inorg. Chem.* **48**, 3467–3479 (2009).
17. Shiddiq, M. et al. Enhancing coherence in molecular spin qubits via atomic clock transitions. *Nature* **531**, 348–351 (2016).
18. Ghosh, S. et al. Multi-frequency EPR studies of a mononuclear holmium single-molecule magnet based on the polyoxometalate $[Ho^{III}(W_5O_{18})_2]^{9-}$. *Dalton Trans.* **41**, 13697–13704 (2012).
19. Alvarez, S., Alemany, P., Casanova, D., Cirera, J. & Llunell, M. Shape maps and polyhedral interconversion paths in transition metal chemistry. *Coord. Chem. Rev.* **249**, 1693–1708 (2005).
20. Frisch, M. J. et al. Gaussian 16 Revision A.03 (Gaussian, 2016).
21. Sarkar, A. & Rajaraman, G. Modulating magnetic anisotropy in Ln(III) single-ion magnets using an external electric field. *Chem. Sci.* **11**, 10324–10330 (2020).
22. Wedge, C. J. et al. Chemical engineering of molecular qubits. *Phys. Rev. Lett.* **108**, 107204 (2012).
23. Kintzel, B. et al. Spin-electric coupling in a cobalt(II)-based spin triangle revealed by electric-field-modulated electron spin resonance spectroscopy. *Angew. Chem. Int. Ed.* **60**, 8832–8838 (2021).
24. Liu, Z. et al. Electric field manipulation enhanced by strong spin-orbit coupling: promoting rare-earth ions as qubits. *Natl Sci. Rev.* **7**, 1557–1563 (2020).
25. George, R. E., Edwards, J. P. & Ardavan, A. Coherent spin control by electrical manipulation of the magnetic anisotropy. *Phys. Rev. Lett.* **110**, 027601 (2013).
26. Mi, X. et al. A coherent spin–photon interface in silicon. *Nature* **555**, 599–603 (2018).

Methods

ESR apparatus and sample configuration. The HoW_{10} crystal was mounted in an ESR quartz tube (outer diameter, 1.6 mm) and inserted between parallel metallized plates separated by 2.0 mm, which were used to apply the *E*-field pulses. Both conductive plates and the sample were mounted in a standard Bruker MD5 resonator and could be independently rotated around the *x* axis, as shown in Fig. 1b. By first studying the CT fields as a function of the sample rotation, we were able to determine the angle between the magnetic easy axis and the experimental rotation axis. In all the experiments presented in this study, the magnetic easy axis was aligned as close as possible to $\mathbf{B}_0$. We applied the *E* field at a variable orientation φ with respect to $\mathbf{B}_0$ (Fig. 1b).

Note that the magnetic easy axis is neither coincident with any of the crystal facets or edges[17,18] nor collinear with the pseudo-fourfold molecular symmetry axis, so it is not possible to guarantee the alignment by inspecting the crystal morphology. Thus, repeating the experiment on a different crystal gives a similar orientation dependence for the SEC, albeit the extrema of the SEC appear at different laboratory directions (see section IV in Supplementary Information). This cosine-shaped orientation dependence of the SEC is indicative of the existence of an axial-type SEC in HoW_{10}. The differences in behaviour between the two crystals arise from the variation in the orientation of crystals in the apparatus and therefore the plane through which they are rotated in the laboratory frame (section V in Supplementary Information provides more details).

Microwave pulse sequences. A standard two-pulse Hahn-echo sequence of duration 2τ ($\pi/2$–τ–π–τ–echo) was employed to measure an electron spin echo on the HoW_{10} crystals. Short broadband pulses, namely, 32 ns for $\pi/2$ pulses and 64 ns for π pulses, were used for measuring the SEC parameters (data shown in Figs. 1 and 2). These pulse parameters were adjusted to optimize the echo intensity. By contrast, long selective pulses, namely, 400 ns for $\pi/2$ pulses and 800 ns for π pulses, were applied in the selective spin manipulation experiments (Fig. 3). These pulse lengths were chosen to excite a narrow frequency population of spins, which can be selectively manipulated using the *E*-field-induced frequency shift, while still giving a reasonable signal-to-noise ratio in spin echo measurements.

Calculation of SEC. The *E*-field-induced change in the CT frequency is evaluated by computing the evolution of the molecular electronic structure using the multireference complete active self-consistent field spin–orbit method (implemented by OpenMolcas[27]) with the combined effect of the crystal field and spin–orbit coupling calculated using the SINGLE_ANISO module[28]. The effect of *E* field on the easy-axis orientation was also estimated (section VIII in Supplementary Information provides more details). The theoretical study was performed using both the obtained crystal structure and the relaxed structure optimized at the DFT level.

Data availability

Experimental data supporting the conclusions are available at https://doi.org/10.5281/zenodo.5167019.

References

27. Fdez. Galvan, I. et al. Openmolcas: from source code to insight. *J. Chem. Theory Comput.* **15**, 5925–5964 (2019).
28. Ungur, L. & Chibotaru, L. F. Ab initio crystal field for lanthanides. *Chem. Eur. J.* **23**, 3708–3718 (2017).

Acknowledgements

This work is supported by the EU (ERC-2014-CoG-647301 DECRESIM, ERC-2018-AdG-788222 MOL-2D, COST Action CA15128 MOLSPIN, the QuantERA project SUMO, and the H2020 research and innovation programme projects SPRING (no. 863098) and FATMOLS (no. 862893)); the Spanish MINECO (grant CTQ2017-89993 co-financed by FEDER and grant MAT2017-89528; the Unit of Excellence 'María de Maeztu' CEX2019-000919-M); the Generalitat Valenciana (Prometeo Program of Excellence); and the UK EPSRC (EP/P000479/1). J.J.B. acknowledges support by the Generalitat Valenciana (CDEIGENT/2019/022). J.M. is supported by Magdalen College, Oxford. J.L. is supported by the Royal Society through a University Research Fellowship.

Author contributions

J.L., E.C., A.G.-A. and A.A. conceived the study. Materials were synthesized by Y.D. under the supervision of E.C. ESR experiments were conducted by J.L. and J.M. Data analysis was performed by J.L. with input from A.A. Theoretical modelling was done by A.U.; assisted by J.J.B.; guided by A.G.-A.; and in discussion with J.L., E.C. and A.A. All the authors contributed to the manuscript.

Competing interests

The authors declare no competing interests.

Additional information

Supplementary information The online version contains supplementary material available at https://doi.org/10.1038/s41567-021-01355-4.

Correspondence and requests for materials should be addressed to Junjie Liu, Alejandro Gaita-Ariño or Arzhang Ardavan.

Peer review information *Nature Physics* thanks Nicholas Chilton, Stergios Piligkos and the other, anonymous, reviewer(s) for their contribution to the peer review of this work.